Supporting Information

Quantitative measurement of red blood cell indices using spectroscopic differential phase-contrast microscopy.

Taegyun Moon [a], Andrew Heegeon Yang [a], Seungri Song [a], Malith Ranathunga[a], Yea-Jin Song [b], Mi-Sook Yang [b], Jaewoo Song [b,*], and Chulmin Joo [a,*]

[a] Department of Mechanical Engineering, Yonsei University, Seodaemoon-gu, Seoul 03722, Republic of Korea

[b] Department of Laboratory Medicine, Yonsei University College of Medicine, Seodaemoon-gu, Seoul 03722, Republic of Korea

* Corresponding authors: LABDX@yuhs.ac and CJOO@yonsei.ac.kr

Table of Contents

1. Color-leakage correction

The LEDs and channels of the camera exhibit a range of spectral emissions and responses; therefore, the light from a color LED can leak into other color channels in the detector. This color leakage severely degrades the image quality, and results in inaccurate phase retrieval. We performed color-leakage correction for the recorded images to enable accurate sDPC phase image reconstruction [1, 2].

The information recorded in the image sensor can be formulated as:

$$\begin{bmatrix} I_R^{CCD} \\ I_G^{CCD} \\ I_B^{CCD} \end{bmatrix} = \begin{bmatrix} R_R^R & R_G^R & R_B^R \\ R_R^G & R_G^G & R_B^G \\ R_R^B & R_G^B & R_B^B \end{bmatrix} \begin{bmatrix} I_R^{IMG} \\ I_G^{IMG} \\ I_B^{IMG} \end{bmatrix}, \quad \text{(s1)}$$

where I_c^{CCD} and I_c^{IMG} are the measured intensity information acquired by the color camera and object intensity information incident on the detector, respectively ($c = R, G, and\ B$). The $3\text{x}3$ matrix in Eq. (s1) describes the crosstalk among the color channels, with the element R_i^j ($i,j = R, G, and\ B$) indicating the response of color channel j of the image sensor to the light of color i.

The color leakage matrix can be experimentally obtained by measuring the RGB pixel values of the sDPC images under the LED light illumination of color i ($i = R, G, and\ B$). Once the color-leakage matrix is obtained, the actual objection information for each color can be obtained by simply performing matrix inversion. Figure S1 shows the results of the color-leakage correction. One can note that the application of color-leakage correction dramatically improves the accuracy of the resultant phase images at each color.

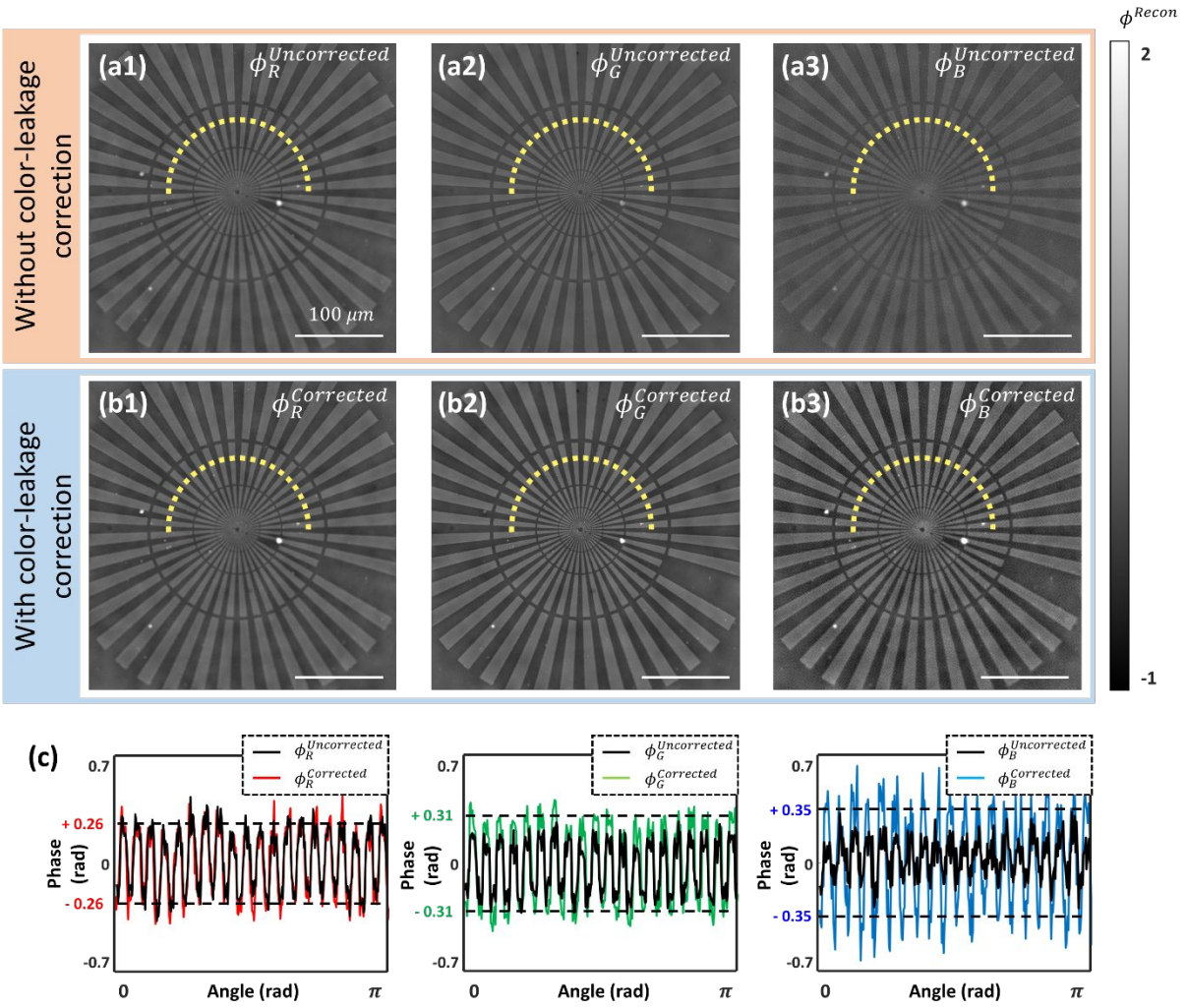

Figure S1. sDPC color-leakage correction results. sDPC phase images of red, green, and blue colors without (a1-3) and with (b1-3) color-leakage correction. (c) Phase information along the yellow dashed lines in (a-b), together with their theoretical estimations (black dashed line). One can note the improved phase accuracy after applying color leakage correction.

2. RBC segmentation

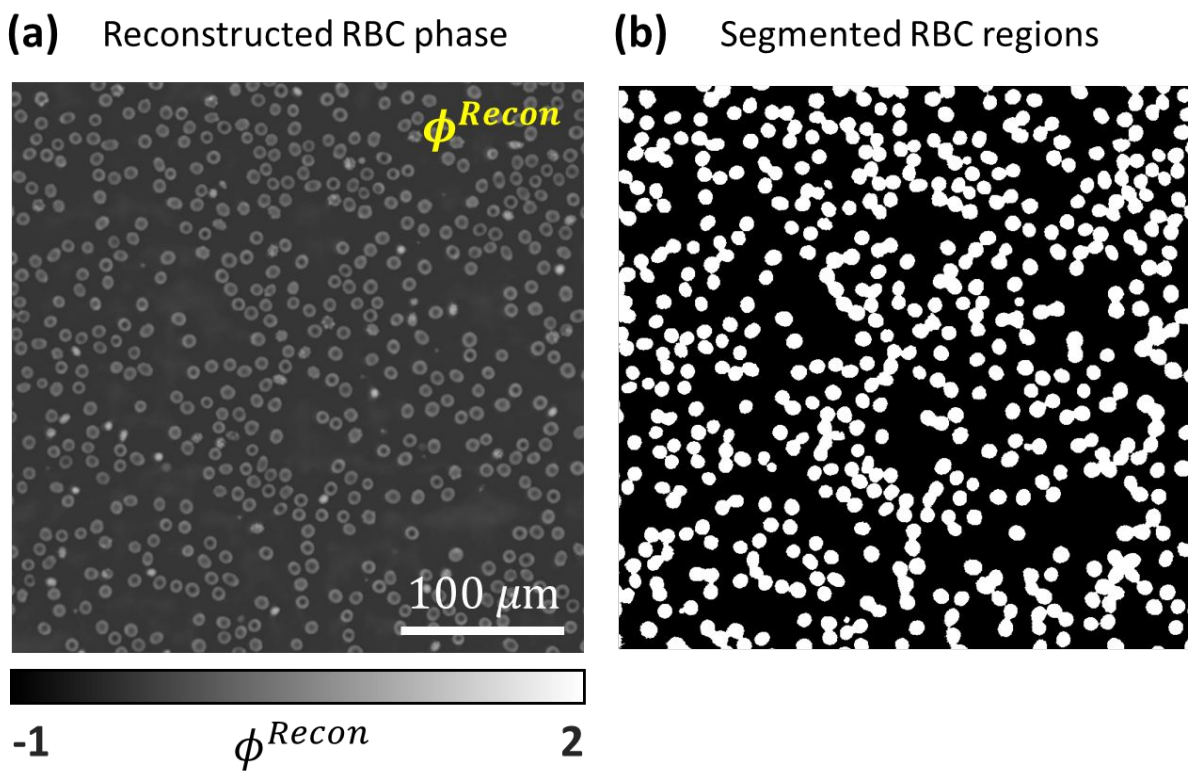

Figure. S2. RBC segmentation. (a) sDPC reconstructed phase image at green color. (b) Segmented RBC region (white region).

We applied the Marker-Controlled Watershed (MCWS) algorithm to segment the RBC areas in the imaging FoV. The MCWS algorithm has been successfully employed to segment RBCs in various imaging studies [3, 4]. The algorithm uses watershed transform and obtains the catchment basin and watershed ridge lines for segmentation [5]. Using the MCWS algorithm applied on the sDPC phase image, segmented RBC areas were found to well match with the RBC areas in the phase image (Figure S2).

3. Polystyrene microbead imaging

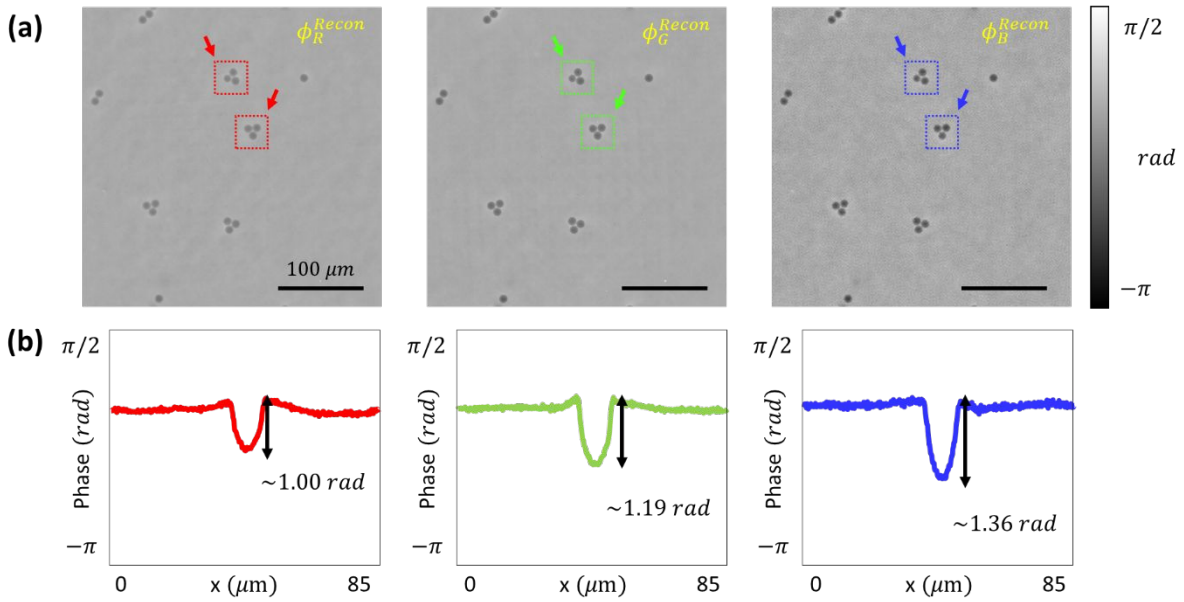

Figure S3. (a) sDPC phase reconstruction of polystyrene microbead at each color R, G, and B. (b) Average line profile of 6 microbeads in the boxed region in (a).

To validate high-accuracy phase imaging capability of our sDPC, we performed imaging of randomly distributed 10 μm polystyrene microbeads (refractive index of $\mathrm{n_{bead}} = 1.59$) immersed in an immersion oil (refractive index of $\mathrm{n_{medium}} = 1.60$). The theoretical phase value of the bead can be calculated as $\Delta\phi_{\mathrm{bead}} = \frac{2\pi}{\lambda}(n_{bead} - n_{medium})\Delta h$, where Δh is thickness of the bead. Note that the estimated phase delays are comparable to those of RBCs (0.997, 1.186, and 1.337 rad for R, G, and B color, respectively). The regularizers were set as the same as in the imaging of Siemens phase target (i.e.$\gamma_{Tik,r} = 7 \times 10^{-4}$, $\gamma_{Tik,g} = 5 \times 10^{-4}$, and $\gamma_{Tik,b} = 3.9 \times 10^{-4}$). The phase delays of the beads relative to the background region were measured to be -1.00, -1.19, and -1.36 rad at R, G, and B colors, respectively, which agreed well with the theoretically estimated phase values with an error of 0.2, 0.8, and 1.7 %.

4. Spatial resolution comparison of coherent QPI and sDPC methods

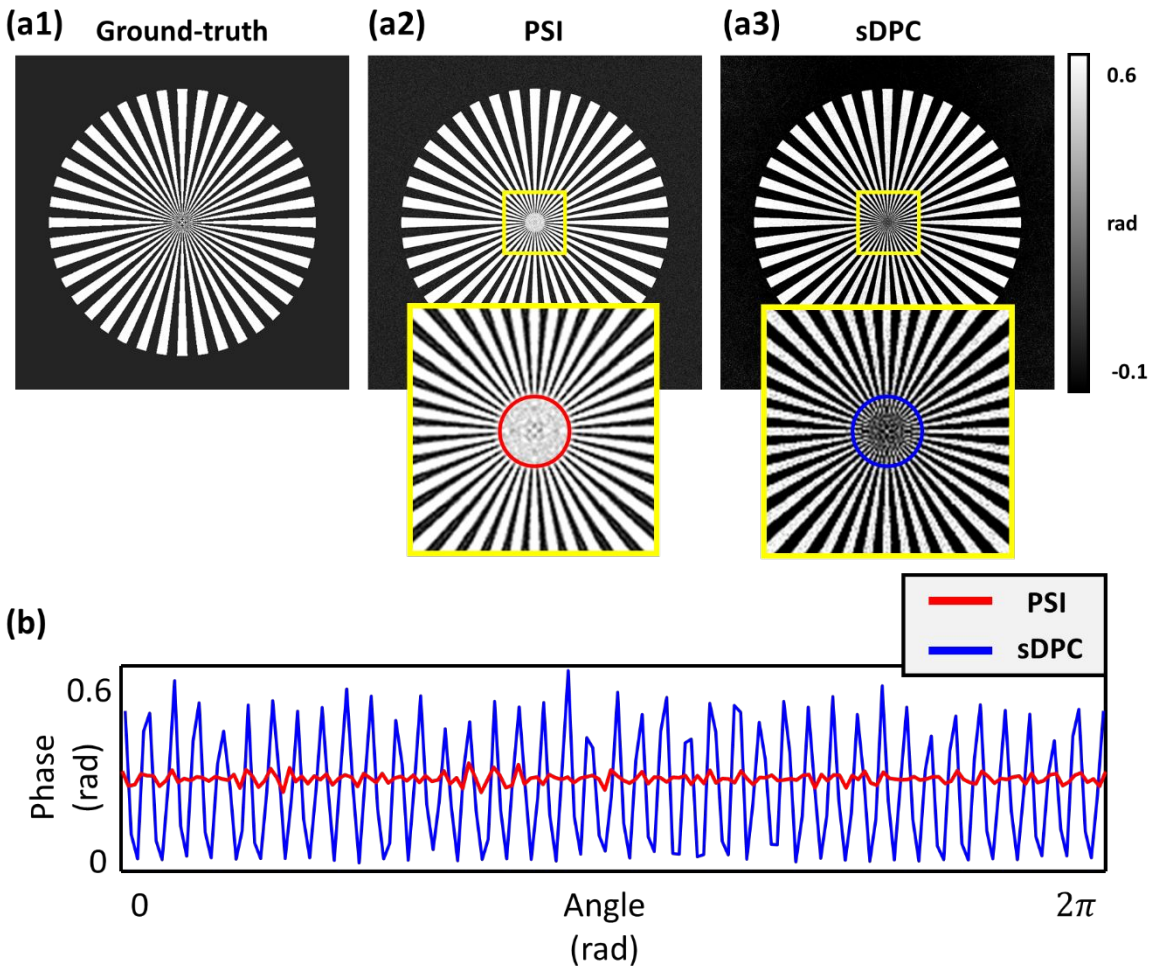

Figure S4. Performed numerical imaging of a spoke phase pattern using a phase-shifting interferometer (PSI) with a coherent light and sDPC. (a1) Ground-truth phase map of the spoke target. Phase reconstruction results with PSI (a2) and sDPC (a3). (b) Phase profiles along the red and blue circles in (a2) and (a3).

To compare the spatial resolutions of coherent QPI and sDPC methods, we performed numerical simulations using a spoke-patterned phase target (Fig. S4(a1)). For coherent imaging, a QPI microscope based on phase shifting interferometry (PSI)[6] was considered with on-axis coherent illumination. In both PSI and sDPC, additive white Gaussian noises with signal-to-noise ratio of 30 dB were imposed for the intensity measurements, and other conditions such as the wavelength and objective NA were identical to the experimental setup. The resultant images are presented in Fig. S4(a2, a3)). It can be noted that sDPC could visualize the spoke patterns with higher spatial frequencies compared to the PSI method. Shown in Figure S4 (b) are the phase profiles along the red and blue circles in Fig. S4 (a2) and (a3), which correspond to the spoke patterns with a spatial frequency of $0.92\ \mu m^{-1}$. The spoke pattern was clearly resolved in the sDPC image, whereas in the PSI phase image, the spoke pattern could not well visualized. We also examined the highest spatial frequencies that can be resolved by PSI and sDPC methods, which were found to be $0.72\ \mu m^{-1}$ and $1.27\ \mu m^{-1}$ for PSI and sDPC methods.

Table S1. Improved sDPC detection performance for RBC indices via the measurements over multiple FoVs

		RBC indices comparison						
		MCHC (g/dl)	MCV (fl)	MCH (pg)	RDW (%)	Hct (%)	Hgb (g/dl)	RBC count $(10^9/mm^3)$
5 FoV	XN-2000	33.7	94.5	31.8	11.6	39.8	13.4	4.2
	sDPC	34.3	93.0	32.1	12.1	38.8	13.4	4.2
	Error	1.9 %	1.6 %	0.8 %	4.7 %	4.5 %	2.1 %	2.9 %

Table S1. RBC indices comparison between the sDPC and automated hematology analyzer (XN-2000). Compared to the detection performance evaluated with 1 FoV measurement (Fig. 4(d)), the relative errors of RDW and RBC were markedly decreased with the measurements over 5 FoVs.

Reference

(1) Lee, W.; Jung, D.; Ryu, S.; Joo, C. Single-exposure quantitative phase imaging in color-coded LED microscopy. *Optics Express* **2017**, *25* (7), 8398-8411.
(2) Lee, W.; Choi, J.-H.; Ryu, S.; Jung, D.; Song, J.; Lee, J.-S.; Joo, C. Color-coded LED microscopy for quantitative phase imaging: Implementation and application to sperm motility analysis. *Methods* **2018**, *136*, 66-74.
(3) Nurçin, F. V.; Imanov, E. Selective Hole Filling of Red Blood Cells for Improved Marker-Controlled Watershed Segmentation. *Scanning* **2021**, *2021*.
(4) Lepcha, P.; Srisukkham, W.; Zhang, L.; Hossain, A. Red Blood based disease screening using marker controlled watershed segmentation and post-processing. In *The 8th International Conference on Software, Knowledge, Information Management and Applications (SKIMA 2014)*, 2014; IEEE: pp 1-7.
(5) Tulsani, H.; Saxena, S.; Yadav, N. Segmentation using morphological watershed transformation for counting blood cells. *IJCAIT* **2013**, *2* (3), 28-36.
(6) Schreiber, H.; Bruning, J. H. Phase shifting interferometry. *Optical shop testing* **2007**, 547-666.